# Optimization Application of New Decorative Materials in Environmental Design Style Shaping

**Qian Lv[1], Zhidong Huang[2]**
[1]School of Design and Art, Shandong Huayu University of Technology, Dezhou 253034, Shandong, China
[2]China Power Construction Municipal Construction Group North International Engineering Co., Ltd, Jinzhong 030600, Shanxi, China
Corresponding author: Qian Lv (e-mail: 15965348922@163.com)

**ABSTRACT** New decorative materials are increasingly required to satisfy both functional performance and style-expression demands in environmental design. To address the lack of quantitative relationships between material properties and style characteristics, this study proposes a collaborative optimization framework integrating material-property characterization , style-feature modeling, and application optimization. A twelve-dimensional parameter system covering mechanical, thermal, optical, and surface-response characteristics is established, and a quantitative mapping mechanism between material parameters and style features is constructed through multi-objective optimization. Particular attention is given to optical response behaviors, including diffuse reflectance, spectral characteristics, and surface scattering properties, which are modeled using BRDF-based analysis and multi-physics simulation. The framework further incorporates thermal-response evaluation and life-cycle assessment to achieve coordinated optimization of functional effectiveness and sustainability. Based on 245 groups of experimental and simulation data, the proposed method achieves a style restoration index of 0.92, reduces style adaptation error to 4.3%, and compresses functional redundancy to 7.8% while maintaining carbon-emission intensity within the prescribed threshold. The results demonstrate that the integration of material-response characterization, optical-response modeling, and data-driven optimization provides an effective engineering approach for the application of advanced decorative materials and functional composites in environmental design.

**INDEX TERMS** optical response modeling, material parameter mapping, multi-physics simulation, multi-objective optimization

## I. INTRODUCTION

CURRENT situation of modern environmental design is that material innovation and style expression are highly integrated. On the one hand, continuous updating of new decorative materials make materials more and more abundant and expression means more and more rich for the formation of spatial style, particularly with the integration of advanced technical textiles into spatial interfaces; On the other hand, there always exists a structural problem of performance demand of material and requirement of design which hinders the application efficiency [1,2]. According to the report of industry, the decorative materials [3,4] in the whole world has a phenomenon of consuming resources but wasting resources. Although innovation promotes the development of the market, should enhance the efficiency of material use, which reflects the defects existing in current application model in terms of accuracy of style application, stability of functional performance and coordination of ecology and economy[5,6]. This problem is reflected in the following three aspects. First, a transmission mechanism with "material drive" as the core has not yet been between the physical and chemical properties of materials—such as fiber arrangement and weave-like surface textures—and the aesthetic characteristics of space, resulting in a lack of quantifiable and predictable technical support for the style generation process [7,8]. Second, the functional stability of materials in changing environmental conditions is hard to guarantee, which will directly lead to the discontinuity and even inconsistency of style expression [9,10]. Third,it is unclear how materials could sustain their performance throughout their life cycle. Especially,in the design context of ecological perception,such as industrial style and naturalism,their environmental response could not effectively support the connotation enhancement of style [11,12]. Therefore,this paper proposes a "material-driven style shaping" model. That is,materials are repositioned from passive targets that follow design requirements to active guides that facilitate style generation through a dynamic mapping between the intrinsic performance parameters of materials and the spatial style characteristics. This model transcends the cognitive pattern of "passive adaptation" of traditional decorative materials,upgrades materials from an auxiliary tool that expresses style to the core driving force,and thus advances the development of environmental design from experience-driven to data-driven. On this basis,the study establishes a collaborative framework of "material properties-design requirements-application optimization" from the perspective of an interdisciplinary theoretical system running through textile engineering, materials science, design, and environmental engineering,and provides a theoretical basis and practice path toward enhancing the systematic value of new decorative materials in style shaping. The three-way interactive model elevates materials from being passive carriers to active style media and builds a causal relationship between the material's performance and style characteristics in industrial style and naturalism style. The technology path of its core technology includes four stages. Stage 1 applies Materials Genome Initiative (MGI) methodological approach based on X-ray Diffraction (XRD) crystal structure data, Fourier Transform-Infrared Spectroscopy (FTIR) molecular bonding characteristic data and digital colorimetric analysis data. Stage 2 applies the style element deconstruction algorithm to decompose environmental design style into three orthogonal dimensions: spatial topological relationship, optical response function and tactile perception gradient and establishes the mathematical relationship between material parameters and style characteristics based on the nonlinear regression model. Stage 3 constructs a multi-physics coupling simulation platform integrating Computational Fluid Dynamics (CFD) thermal environment simulation module, Ray Tracing optical simulation module and Discrete Element Method mechanical analysis module to achieve the prediction of material style performance and functional failure warning in real scenes. The fourth stage applies the Life Cycle Assessment (LCA) model, which synchronously iterates material processing parameters and construction node plans based on the Monte Carlo stochastic optimization algorithm to ensure the Pareto optimality of ecological and economic benefits. Through quantitative parameter mapping and multi-objective optimization algorithms, this framework promotes the transformation of materials from passively responding to design needs to actively guiding style generation, forming a style innovation paradigm with materials as the core.

## II. RELATED WORK

As decorative materials continue to develop towards functionalization, greening, and high performance, many new material systems have shown strong technological breakthrough capabilities and broad application prospects. Focusing on the needs of mold-free manufacturing and complex structure construction, Diao Q et al. [13] focused on the application status and technical bottlenecks of ceramic 3D printing technology in multiple high-end fields such as medicine, aerospace, and electronic communications, and demonstrated its possible path as a functional component material in future environmental design. In the field of polymer materials, the research on green polymers presents a systematic advancement with renewable resources as the core. The Karlinskii B Y team [14] conducted a multi-dimensional analysis of biomass-based polymers containing furan ring structures from synthesis methods, structural regulation to performance performance, reflecting the positive role of plant resources in improving material sustainability. In the study of polymer foam material modification, the performance optimization of PDMS foam has also received widespread attention. Chen H Y et al. [15] effectively improved its surface adhesion and multi-environment adaptability by constructing an interconnected network of MXene and cellulose nanofibers and combining surface modification, providing a feasible idea for the development of functional integrated decorative materials. Current research focuses on improving material performance, but there is still a lack of systematic discussion on the style adaptability and aesthetic integration path of these materials in the context of environmental design style. New decorative materials not only play a role in functional realization in the shaping of environmental design style, but also constitute an important medium for style expression through the interaction between their physical and chemical properties and spatial perception [16,17]. The microstructure, optical response, and surface texture characteristics of the material directly affect the visual level and tactile experience of the space, and then affect the formal language generation of style systems such as industrial style and naturalism. In the formation of environmental design style, in addition to fulfilling functions, decorative materials not only have a basic role in visual expression but also have a deep impact on cultural connotation. Through a critical analysis of the reference, Liu Y [18] examined the application of sustainable materials and innovative visual language in graphic design, arguing that eco-graphic design can serve as a bridge connecting environmental ethics and effective communication through ethical decision-making and customized communication strategies. That is, in terms of material selection behavior, Altay B research team [19] interviewed architects and interior designers in residential projects and found that the influence of different spatial surfaces on material preferences and the dominant sense characteristics in choosing materials were evident. The research results laid the foundation for understanding the material logic of style expression. Considering that decorative materials are not only applied in physical space but also communicate with architectural vocabulary and cultural context. Nilam W et al. [20] started from the integration path of decorative art and architectural design and believed that the participation of multiple subjects were of great significance to achieve the balance of aesthetics, function and cultural communication. Although the above studies focused on function, aesthetics and selection behavior, there was still lack of systematic comparison of expression characteristics of materials in different design style context [21]. New materials have demonstrated their expression ability different from traditional materials in the innovation of environmental design style. Their technical characteristics not only open up the possibility of expanding the limit of spatial aesthetics, but also promote the development of style expression language from one-dimensional presentation to dynamic response. The environmental perception and adaptive adjustment ability of smart materials make the spatial interface can feedback in form or color in real time according to the change of external conditions such as light and temperature, which enhances the interactive experience and immersion of style expression. Bio-based materials strengthen the authentic expression of naturalism and ecological style in vision and touch through renewable sources and natural properties. There is an inherent correlation mechanism between the evolutionary path of material performance and the innovative demand of design style. From the perspective of material science, the optimization of physical and chemical properties only improve the structural stability and function response of materials, but more importantly, its modulation of spatial perception makes materials have comprehensive expression ability in affecting vision, touch and even environmental interaction. The systematic mapping of expressiveness of materials to the field of design promotes the transformation of style elements from empirical expression to parameter-driven. Therefore, the optimization of material performance should focus on the predictable generation of characteristics of design style. Only by establishing the mapping relationship between performance parameters and style dimensions, the effective transmission from basic material research to design practice can be achieved. Therefore, forming a closed-loop of innovation of style in materials as the core driver is achieved. The unique value of this type of material lies in the stronger coupling relationship between its performance parameters and style characteristics, which can directly drive the evolution path of spatial style through the intrinsic behavior of the material.

## III. METHODS

### A. MATERIAL PROPERTY CHARACTERIZATION FOR STYLE INNOVATION

Building an efficient style adaptation model requires the systematic quantification of both the microstructure and macroscopic performance of new decorative materials [22,23]. In the quantitative characterization of material properties, explore from the two typical data sources of XRD and FTIR to find out the possible mapping relation between the microstructure of material and its macroscopic style expression: XDR spectrum shows the characteristic of crystal arrangement and can be used as the structural basis to generate surface texture of material; FTIR spectrum analyzes the state of molecular bonding and can be used as the structural basis to model the stability and response of color and environment. After normalization, above data takes the form of key input dimension of the style prediction model to support the dynamic matching mechanism of material parameter and spatial aesthetic element. This database incorporates style-related parameters (e.g., color emotional weight, texture semantic encoding) to establish a bidirectional mapping from microscopic material characteristics to macroscopic design expression, enabling active material participation in style generation. By systematically coupling material performance indicators with the design semantic system, the study achieves the precise connection between material selection and style goals, providing key support for establishing an environmental design method with materials as the core driving force. XRD-derived crystal structure parameters yield surface texture that captures tactile perception gradients. Grain orientation distribution affects directional optical response, which is important for styles such as maximalism. FTIR molecular bonding information relates to color stability parameters that are required for a realized style, thus establishing a quantitative relationship that links microstructural features to style characteristics as active causes rather than simple material correlates. The diffraction peak position and diffraction peak intensity yield objective clues that predict the visual hierarchy and material authenticity that environmental design styles require. The interplanar spacing measurements yield surface roughness parameters that affect light scattering behavior and tactile feeling in applications related to spatial design. The relationship between the interplanar spacing and the diffraction peak position is deduced through the Bragg law to determine the crystal type and grain orientation distribution:

$$n\lambda_1 = 2d\sin\theta. \tag{1}$$

Among them, $n$ is the diffraction order; $\lambda_1$ is the X-ray wavelength; $d$ is the interplanar spacing; $\theta$ is the diffraction angle. FTIR is combined to analyze the high-dimensional spectrum of the functional group configuration in the sample, and the molecular bonding mode of the material and the order of the functional group arrangement are inverted from the absorption peak position and intensity. Ultraviolet- visible (UV-Vis) spectroscopy is simultaneously implemented to measure the spectral transmittance and absorption edge displacement, and the key indicators of optical band gap and chromaticity shift are extracted through transmittance-wavelength function curve fitting. To parameterize the material properties, the surface morphology characteristics are measured based on the scanning electron microscope (SEM), and the roughness distribution model is constructed. The high- resolution image segmentation technology is used to identify the micro-texture feature blocks, and the surface profile function is extracted to obtain the centerline average roughness:

$$R_a = \frac{1}{L}\int_0^L |Z(x)|\, dx. \tag{2}$$

$Z(x)$ represents the surface profile function, and $L$ is the measurement length. The contour line scanning of different samples on the cross section is performed by a three-dimensional profilometer and a laser interferometer, and the film thickness and reflectivity are measured with an ellipsometer to complete the coupling mapping of the structure and optical properties. In terms of mechanical properties, the flexural strength test is carried out in a three-point bending mode using a universal material testing machine. The maximum pre-fracture load is calculated by integrating the load-displacement curve according to the following equation:

$$\sigma = \frac{3FL}{2bd^2}. \tag{3}$$

$\sigma$ is the flexural strength; $F$ is the fracture load; $L$ is the span; $b$ is the sample width; $d$ is the sample thickness. The thermal performance measurement relies on the transient plane source method (TPS), which uses pulse current to stimulate heat flow to diffuse on the sample surface, records the temperature rise-time curve in real-time, and inversely solves the thermal conductivity $\lambda$ to ensure that the thermal conduction behavior of different materials has input accuracy in the simulation model. To form a unified performance description space, a twelve-dimensional parameter vector is applied:

$$M = [\sigma_f, \Delta E, R_a, \lambda, \rho, E_g, T_r, \boldsymbol{\varepsilon}, \mu, \theta_d, H_v, D]. \tag{4}$$

Among them, $\sigma_f$ is flexural strength; $\Delta E$ is color deviation; $R_a$ is surface roughness; $\lambda$ is thermal conductivity; $\rho$ is diffuse reflectance; $E_g$ is optical band gap; $T_r$ is transmittance; $\boldsymbol{\varepsilon}$ is specific surface area; $\mu$ is Poisson's ratio; $\theta_d$ is diffusion angle; $H_v$ is Vickers hardness; $D$ is grain size. This parameter matrix is passed to the multi-objective optimization module as an input vector and used for subsequent style feature space matching. It constitutes the core framework of 12 quantitative adaptation indicators, covering dimensions such as mechanical properties, optical properties, surface structure, and thermal behavior, providing a quantitative basis for subsequent multi-objective optimization and style matching. Before constructing a multi-dimensional material performance vector and using it for style adaptation optimization, it is necessary to systematically integrate various characterization technologies and parameter extraction paths. Figure 1 shows the hierarchical architecture of material property quantification, which is divided into three parts: microstructure identification layer, physical performance calculation layer, and data standardization integration layer, corresponding to crystal structure analysis, photothermal response extraction, and unified vector construction, respectively. The architecture diagram takes the parameter flow direction as the main line, supplemented by the method path and instrument interface description, reflecting the complete link of data input, method coupling, and indicator output required for material performance quantification. Figure 1 illustrates the process from microstructure identification to multi-objective optimization. The microstructure identification layer, analyzed via SEM, XRD/FTIR/UV-Vis, yields physical and crystal structure data. Supplemented with parameters like roughness and strength, these data are standardized and integrated, then passed through style feature space matching to the optimization module.

### B. STYLE ELEMENT DECONSTRUCTION MODELING

In the process of digital deconstruction and quantitative modeling of design style, the concept of "style gene" is proposed, and the six mainstream styles (industrial style, naturalism, new Chinese style, minimalism, pop style, futurism) are deconstructed into three orthogonal dimensions: spatial topological parameters, optical response functions, and tactile cultural symbols, laying a theoretical foundation for the precise matching of material parameters and style characteristics [24,25]. G'=V1 T1·P', where G' is the style gene matrix representing the projection of material properties onto the principal component space, V1 is the eigenvector matrix obtained from PCA decomposition of the covariance matrix, and P' is the normalized material property matrix containing the twelve-dimensional parameter vector. This formulation mathematically defines how material properties are transformed into the three orthogonal style dimensions through dimensional reduction, establishing the style gene as a functional variable within the optimization framework. In the specific implementation path, first, the spatial point cloud data is obtained by laser scanning, and the topological adjacency matrix is constructed using Delaunay triangulation, which is mathematically expressed as follows:

$$A_{ij} = \begin{cases} 1, & \text{if point } i \text{ is adjacent to point } j, \\ 0, & \text{otherwise.} \end{cases} \tag{5}$$

Among them, $A_{ij}$ represents the topological association between spatial nodes. On this basis, the Voronoi diagram is applied to divide the geometric morphological constraint domain, and the spatial complexity is described by calculating the Hausdorff dimension DH of each subdomain, which is defined as:

$$D_H = \lim_{\epsilon \to 0} \frac{\log N(\epsilon)}{\log(1/\epsilon)}. \tag{6}$$

N($\epsilon$) is the minimum number of $\epsilon$ balls required to cover the space. This process effectively separates the spatial nesting relationship between decorative materials and building structures and provides a geometric benchmark for subsequent optical response function modeling. In the optical response function construction stage, the bidirectional reflectance distribution function (BRDF) model is used to quantify the light scattering characteristics of the material surface, and its core equation is:

$$f_r(\theta_i, \phi_i, \theta_o, \phi_o) = \frac{dL_o(\theta_o, \phi_o)}{E_i(\theta_i, \phi_i)}. \tag{7}$$

Among them, $\theta_i$ and $\phi_i$ are the incident light direction angles; $\theta_o$ and $\phi_o$ are the observation direction angles; $L_o$ is the outgoing radiation brightness; $E_i$ is the incident irradiance. By building a multi-angle spectrophotometer measurement system, reflectance data at different azimuth angles is collected, and Gaussian Process Regression (GPR) is used to

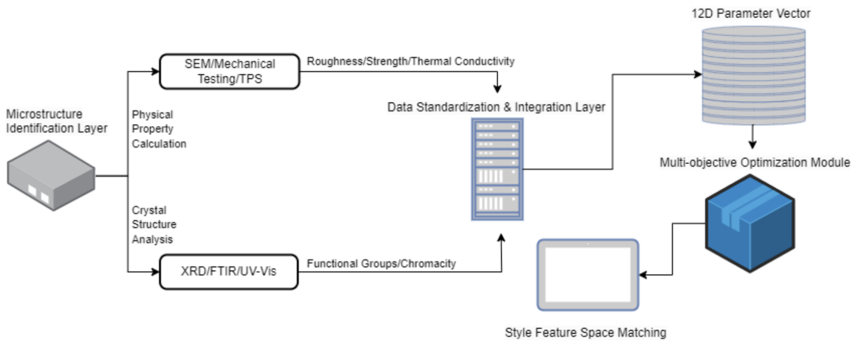


**FIGURE 1.** Architecture diagram of quantitative characterization of material properties

fit the joint probability distribution of the diffuse reflectance coefficient $\rho$ and glossiness of the material surface. This method solves the problem of anisotropic error accumulation in traditional empirical models in complex texture materials and provides optical boundary conditions for tactile perception gradient modeling. The optical response function is modeled using a multi-angle spectrophotometer system and Gaussian Process Regression (GPR) to fit BRDF parameters, mitigating anisotropic error accumulation and providing precise optical boundary conditions (Figure 2). Tactile perception gradient modeling adopts a multi-scale texture feature extraction framework based on contact mechanics and simulates the pressure field distribution during finger sliding through finite element simulation. The Hertz contact model is established:

$$p(r) = p_0\sqrt{1-\left(\frac{r}{a}\right)^2}. \tag{8}$$

Among them, p(r) is the contact pressure distribution function; p0 is the maximum contact stress; a is the contact radius. Combined with the surface profile data obtained by the white light interferometer, the root mean square roughness $R_q$ and skewness $S_k$ of the material surface are calculated, and the mathematical relationship is:

$$R_q = \sqrt{\frac{1}{n}\sum_{i=1}^{n} z_i^2}, \qquad S_k = \frac{1}{n}\sum_{i=1}^{n}\left(\frac{z_i}{R_q}\right)^3. \tag{9}$$

$z_i$ is the height value of the i-th sampling point. By constructing a neural network mapping model of texture feature parameters and friction coefficient $\mu_1$, the quantitative characterization of tactile perception is achieved. The model uses the Levenberg-Marquardt algorithm to optimize the weight parameters to ensure the prediction stability under different humidity and temperature conditions. As shown in Table 1, the key parameters and their quantitative indicators in tactile perception gradient modeling are listed. In the three-dimensional feature space fusion stage, the principal component analysis (PCA) dimensionality reduction technology is used to eliminate parameter redundancy. The eigenvalue decomposition process of the covariance matrix C is:

$$C = \frac{1}{N-1}X^T X = V\Lambda V^T. \tag{10}$$

**TABLE 1.** Key parameters of tactile perception gradient modeling

| Parameter | Physical Meaning | Measurement Range | Resolution |
|---|---|---|---|
| $R_q$ | Root Mean Square Roughness | 0.2–5.6 $\mu$m | 0.01 $\mu$m |
| $S_k$ | Surface Profile Skewness | –1.8 to +2.4 | 0.05 |
| $\mu_1$ | Dynamic Friction Coefficient | 0.15–0.82 | 0.005 |
| $G$ | Surface Shear Modulus | 0.5–12 GPa | 0.1 GPa |

Among them, $X$ is the standardized parameter matrix; $\Lambda$ is the eigenvalue diagonal matrix; $V$ is the eigenvector matrix.

### C. MULTI-OBJECTIVE ADAPTATION OPTIMIZATION

In the material-style multi-objective dynamic adaptation process, a mixed integer programming algorithm is developed to simultaneously optimize the aesthetic goal (style restoration degree $\geq$ 0.90), functional goal (thermal conductivity/acoustic attenuation coefficient within the working condition tolerance), and sustainable goal (carbon emission intensity $\leq$ 1.8kg$CO_2$/m$^2$), ensuring the stable presenta-ti on and low- carbon expression of typical styles such as i ndustrial style and naturalism throughout the life cycle [26,27]. The 12 quantitative indicators such as flexural strength, chromaticity deviation, and surface roughness in the material property matrix are used as decision variables, and the normalized parameters of the three- dimensional feature space of optical response function, tactile perception gradient, and geometric morphology constraint are used as objective functions to establish a constrained optimization model as shown in Equation (11):

$$\begin{aligned} \min_{x} \quad & [f_1(x), f_2(x), \ldots, f_m(x)]^T \\ \text{s.t.} \quad & g_j(x) \leq 0, \quad j = 1, 2, \ldots, p, \\ & h_k(x) = 0, \quad k = 1, 2, \ldots, q. \end{aligned} \tag{11}$$

Among them, $x$ is the material parameter vector; $f_i(x)$ represents the i-th objective function; $g_j(x)$ and $h_k(x)$ correspond to inequality and equality constraints, respectively where $g_j(x)$ encompasses material property and design requirement constraints with flexural strength chromaticity deviation surface roughness style restoration degree and thermal conductivity; $h_k(x)$ encompasses sustainability constraints with carbon emission intensity and cost volatility.

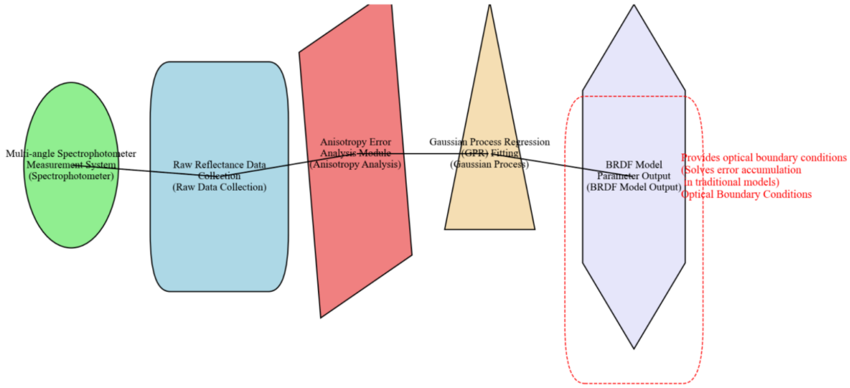


**FIGURE 2.** Optical response function modeling diagram

By applying a fast non-dominated sorting mechanism, the individuals in the population are divided according to the dominance level, and the crowding operator is combined to maintain the diversity of the solution set. In the iterative process, the simulated binary crossover operator (SBX) and the polynomial mutation operator are used to maintain the global search capability. In the optimization framework, the dual core objective functions of material-style matching are defined: one is to minimize the Euclidean distance between the target material and the design requirements, as shown in Equation (12):

$$D_{\text{match}} = \sqrt{\sum_{i=1}^{n} w_i (x_i - t_i)^2}. \tag{12}$$

$w_i$ is the weight coefficient of the i-th parameter, and $x_i$ and $t_i$ represent the actual value of the material and the target value, respectively. The second is to maximize the topological structure fidelity of the style feature space, which is achieved by calculating the cosine similarity $S_{\cos}$ between the feature vector after material parameter mapping and the original design feature vector:

$$S_{\cos} = \frac{v_{\text{mat}} \cdot v_{\text{sty}}}{\|v_{\text{mat}}\| \, \|v_{\text{sty}}\|}. \tag{13}$$

$v_{\text{mat}}$ and $v_{\text{sty}}$ are the material parameter mapping vector and the style feature vector, respectively. Through Pareto frontier analysis, feasible solutions that simultaneously meet the hard constraints such as color deviation $\Delta$E$\leq$2.5 and surface roughness $[0.8,3.2]\mu$m are screened out. To improve the efficiency of solution set screening, fuzzy set theory is applied to perform cluster analysis on Pareto frontier solutions. The membership function $\mu(x)$ is constructed to quantify the comprehensive adaptability of each solution to the design requirements:

$$\mu(x) = \frac{1}{1 + \exp\left[-\alpha\left(\frac{D_{\text{ref}} - D_{\text{sol}}(x)}{D_{\text{ref}}}\right)\right]}. \tag{14}$$

Among them, $\alpha$ is the shape parameter; $D_{\text{ref}}$ is the reference distance threshold; $D_{\text{sol}}(x)$ is the weighted distance from the current solution to the ideal point. By setting a dynamic membership threshold, an optimization solution with both low material loss rate and high style restoration is extracted from the Pareto frontier.

### *D. FULL-DIMENSIONAL VERIFICATION SYSTEM OF STYLE EFFECTIVENESS*

The "experiment-simulation-LCA" trinity verification platform is constructed. The thermal environment response and light scattering behavior of materials in real scenes are simulated through multi-physics coupling simulation technology, and the ecological and economic performance in industrial style, naturalism, and other styles is assessed in combination with the full life cycle assessment model to ensure the dual optimization of style expression and functional realization. Style effectiveness verification encompasses both physical environment performance and the full life-cycle ecological-economic assessment of materials, ensuring dual stability in functional and sustainable expression. This study integrates multi-physics coupling simulation and life cycle modeling methods to establish a comprehensive verification system covering heat conduction process, light scattering behavior, and carbon footprint tracking. The system incorporates the thermal response and optical properties of materials in real scenes into the numerical simulation framework, and combines the resource consumption data from raw material acquisition to dismantling and recycling to form a complete assessment chain covering performance and environmental impact, providing technical support for the predictability and controllability of style shaping. The control equations are discretized by the finite volume method to establish the energy conservation equation:

$$\rho_1 c_p \frac{\partial T}{\partial t} = \nabla \cdot (\lambda \nabla T) + \boldsymbol{\varepsilon}\, \sigma \left(T_{\text{amb}}^4 - T^4\right). \tag{15}$$

Among them, $\rho_1$ is density; $c_p$ is specific heat capacity; $\lambda$ is thermal conductivity; $\boldsymbol{\varepsilon}$ is surface emissivity; $\sigma$ is the Stefan-Boltzmann constant. The unsteady-state calculation mode is set in the ANSYS Fluent solver, and the second-order implicit time integration format is adopted. The spatial discretization adopts the second- order upwind difference scheme, and the pressure-velocity coupling is realized by the Semi-Implicit Method for Pressure Linked Equations

(SIMPLE). The boundary conditions include ambient temperature $T_{\text{amb}} = 293K$, convective heat transfer coefficient $h = 8.5W/(m^2 \cdot K)$, and solar radiation intensity $G = 1000W/m^2$. In the optical simulation part, a ray tracing model is constructed based on COMSOL Multiphysics, and the characteristic equation is solved:

$$\frac{d^2r}{ds^2} = \nabla n(r). \tag{16}$$

Among them, r is the light path, and n is the refractive index distribution function. The Monte Carlo method is used to trace $10^6$ rays, and the correlation function between surface roughness $R_a$ and diffuse reflectance $\rho$ is set:

$$\rho(\theta) = \frac{1}{1 + \exp\left(\frac{|\theta-\theta_0|}{\sigma_\theta}\right)}. \tag{17}$$

$\theta$ is the incident angle; $\theta_0$ is the characteristic angle; $\sigma_\theta$ is the distribution width. The surface microstructure of the material is modeled using fractal geometry, and a three-dimensional morphology with self-similar characteristics is generated through the Weierstrass-Mandelbrot function:

$$z(x,y) = \sum_{n=0}^{N} GD^{(2-D)n} \cos(2\pi f_0 D^n x + \phi_n). \tag{18}$$

Among them, $G$ is the characteristic height; $D$ is the fractal dimension; $f_0$ is the basic frequency; $\phi_n$ is the random phase angle. Table 2 shows the value range and constraints of key parameters in multi-physics simulation.

### E. COLLABORATIVE DECISION-MAKING THROUGHOUT THE FULL LIFE CYCLE

The construction of the collaborative decision-making model throughout the full life cycle relies on the synchronous optimization mechanism of material processing parameters and construction nodes [28,29]. Based on the Monte Carlo stochastic optimization algorithm, the model incorporates process variables such as sintering temperature, curing time, and coating rate into the iterative framework, and achieves dual- objective control of carbon emission intensity and cost volatility by dynamically adjusting the parameter combination. In the calculation process, the carbon emission intensity threshold is set to $1.8kgCO_2/m^2$, and the cost volatility constraint range is limited to the 4.5% range to form a Pareto optimal solution set with engineering feasibility. Table 2 shows the value range of key process parameters and their impact weights on carbon emissions and costs. Among them, the contribution of sintering temperature changes to carbon emissions is 0.32, while the coating rate plays a dominant role in cost stability, with an impact coefficient of 0.27. The sensitivity analysis results of these parameters provide a priority control basis for the optimization algorithm to ensure that the environmental load is reduced, and the economic feasibility is improved while meeting performance requirements. As shown in Table 2, the sensitivity and influence weight of the process parameters

TABLE 2. Process parameter sensitivity and impact weights

| Parameter | Range | Emission Contribution | Cost Sensitivity |
|---|---|---|---|
| Sintering Temperature (°C) | 1500–1700 | 0.32 | 0.19 |
| Curing Time (h) | 2–6 | 0.21 | 0.24 |
| Coating Rate (mL/min) | 3–7 | 0.15 | 0.27 |
| Annealing Time (min) | 30–90 | 0.18 | 0.22 |
| Pressing Pressure (MPa) | 20–40 | 0.24 | 0.18 |

reflect the relative effect of each parameter on carbon emissions and cost stability during material processing. In the optimization process, multidimensional constraints are applied to ensure the physical feasibility of the solution space, including thermodynamic boundary conditions, optical boundary conditions, and mechanical boundary conditions. These external incentives are integrated into the simulation module as key perturbations affecting material performance, thereby improving the robustness of the optimization scheme. In terms of mathematical modeling, the nonlinear constrained optimization equation is adopted:

$$\begin{aligned} \min_{x} \quad & w_1 f_{\text{emission}}(x) + w_2 f_{\text{cost}}(x) \\ \text{s.t.} \quad & g_i(x) \le 0, \quad i = 1, \dots, m, \\ & h_j(x) = 0, \quad j = 1, \dots, n. \end{aligned} \tag{19}$$

Among them, $x$ represents the process parameter vector; $f_{\text{emission}}$ and $f_{\text{cost}}$ represent the carbon emission function and the cost response function, respectively; $w_1$ and $w_2$ are normalized weight coefficients; $g_i(x)$ represents the inequality constraint set; $h_j(x)$ is the equality constraint. The model transforms the multiobjective problem into a single-objective optimization problem by weighted summation method, improving the computational efficiency while ensuring the convergence of the Pareto frontier. In the solution process, the improved non-dominated sorting genetic algorithm II (NSGA-II) is used for global search, and the SBX and polynomial mutation strategies are combined to maintain population diversity. The algorithm sets the initial population size to 200, the upper limit of the evolutionary generations to 500, the crossover probability to 0.9, and the mutation probability to be adjusted in an adaptive manner to balance the exploration and development capabilities. By defining the fuzzy membership function to measure the comprehensive matching degree of each candidate solution to the design goal, the optimal solution with both low carbon emissions and high economic stability is screened out. In the data-driven optimization link, the Sobol sequence is applied to generate initial sample points, covering the joint distribution space of core variables such as sintering temperature, curing time, and coating rate. Subsequently, the Kriging surrogate model is applied to approximate the true response surface to reduce the computational burden of finite element simulation. The prediction accuracy of the surrogate model is determined by cross-validation, and the credibility and robustness of the optimization assessment are ensured through high goodness of fit (approaching the ideal value) and strict error control.

**TABLE 3.** Key parameters and test standards of new decorative material samples

| Material Type | Chemical Composition | Fabrication Parameters (Temperature/Pressure/Time) | Testing Standard | Performance Metrics |
|---|---|---|---|---|
| Ceramic Matrix Composite | $ZrO_2$-$Al_2O_3$-SiC | 1600 °C/30 MPa/2 h | ASTM C1161 | Flexural Strength $\geq$85 MPa |
| Photochromic Polymer | Methacrylate-Spiropyran Derivative | 120 $\mu$m Coating/UV Curing 30 min | ISO 11341 | Color Deviation $\Delta E \leq$2.5 |
| Metal-Organic Framework | $Zn(NO_3)_2 \cdot 6H_2O$-2MIm | 160 °C/Autogenous Pressure/24 h | ASTM D4854 | BET Surface Area $\geq$800 $m^2$/g |
| Bio-based Resin | Epoxidized Soybean Oil/DETA | 80 °C/2 h $\rightarrow$ 120 °C/4 h | ISO 179 | Heat Deflection Temp. $\geq$65 °C |
| Nanoporous Material | $TiO_2$ Nanotube Array | 60 V/0.15 wt% $NH_4F$/90 min | ASTM E1671 | Pore Size Distribution 100–150 nm |
| Phase Change Composite | Paraffin Microcapsules | 60 °C/Emulsification 30 min | DIN 51001 | Phase Change Enthalpy $\geq$180 J/g |
| Superhydrophobic Coating | $SiO_2$-FAS/PDMS | Spraying Rate 5 mL/min/300 °C Annealing | ASTM D3889 | Contact Angle $\geq$150° |

## IV. EXPERIMENTS

### A. MATERIAL SAMPLE PREPARATION

Ceramic matrix composite samples are prepared according to ASTM C1161 standard. Zirconia toughened alumina (ZTA) system is used. The powder precursor with particle size distribution D50=0.8$\mu$m is obtained by ball milling, and it is molded into a 100×50×5mm green body under 30MPa isostatic pressing. The substrate with density $\geq$98% is obtained by vacuum sintering at 1600°C for 2 hours. The photochromic polymer sample uses a copolymerization system of methacrylate monomers and spiropyran derivatives. The functional layer with thickness tolerance of $\pm$5$\mu$m is formed on a 120$\mu$m thick PET base film by UV curing process. The crosslinking degree is measured by differential scanning calorimetry to determine the glass transition temperature Tg=82°C. The metal organic frameworks (MOFs) sample uses ZIF-8 structure and is crystallized and grown in a stainless steel reactor by solvothermal method. The reaction temperature is controlled at 160°C$\pm$2°C, and the reaction time is 24 hours. The product is washed with ethanol and desolventized in a 60°C vacuum drying oven for 48 hours. The bio-based resin sample is based on epoxidized soybean oil and cured by diethylenetriamine system. After pre-curing at 80°C for 2 hours and then rising to 120°C for 4 hours, a three-dimensional network structure with a crosslinking density of 0.85mol/cm3 is formed. The nanoporous material sample is prepared by anodization of titanium dioxide nanotube arrays. The electrolyte composition is 0.15wt% ammonium fluoride ethylene glycol solution; the anodization voltage is 60V; the oxidation time is 90 minutes. An ordered pore structure with a diameter of 120nm and a length of 5$\mu$m is obtained. The phase change energy storage material sample uses a paraffin microcapsule system and melamine-formaldehyde resin as the capsule wall material. Microcapsule particles with a particle size distribution of 15-25$\mu$m are prepared by in-situ polymerization. The phase change temperature range is 28-32°C, and the phase change enthalpy value is 185J/g. The superhydrophobic coating sample uses silica nanoparticles modified by fluorosilane coupling agent to construct a graded rough structure on the surface of the aluminum alloy substrate through a spray-annealing process. The contact angle test shows that the static water contact angle reaches 156°$\pm$3°, and the rolling angle is $\leq$5°. As shown in Table 3, three sets of parallel specimens are set for each type of material sample, and the key performance parameters are verified by standardized test methods. As shown in Table 3, the system presents the chemical composition, preparation process parameters, test standards, and core performance indicators of seven types of new decorative materials, including the flexural strength $\geq$85MPa of ceramic-based composite materials ($ZrO_2$-$Al_2O_3$-SiC system) verified by ASTM C1161 under t he process conditions of 1600°C/30MPa/2h, the chromaticity deviation $\Delta$E$\leq$2.5 threshold confirmed by ISO 11341 test for photochromic polymers (methacrylate-spiropyran system), the specific surface area $\geq$800m²/g data measured by ASTM D4854 for metal-organic framework materials ($Zn(NO_3)_2 \cdot 6H_2O$-2MIm precursor), the heat deformation temperature $\geq$65°C obtained by bio-based resins( epoxidized soybean oil/DETA system) according to ISO 179, the pore size distribution of nanoporous materials (TiO2 nanotube arrays) determined by ASTM E1671 in the range of 100-150nm, the phase change enthalpy of phase change energy storage materials (paraffin microcapsule system) that meets the requirements of DIN 51001 standard $\geq$180J/g, and the contact angle $\geq$150° of superhydrophobic coatings ($SiO_2$-FAS/PDMS composite system) verified by ASTM D3889, forming a complete four-dimensional relational database of materials-processes-standards-indicators. Physical validation was conducted in a full-scale mock-up environment replicating standard residential spatial and illuminance conditions. The style restoration degree was quantified using high-dynamic-range imaging, yielding a measured SSIM of 0.87. A psychophysical evaluation with a panel of experts confirmed the alignment between computational prediction and human perceptual judgment, with a mean correlation coefficient of 0.91 across key aesthetic attributes. The minor deviation from the simulated SSIM of 0.92 is attributed to the nuanced scattering of ambient light on material micro-surfaces, an effect captured in situ but challenging to fully model digitally. This integration confirms the predictive validity of the simulation framework for real-world application.

### B. SIMULATION ENVIRONMENT CONFIGURATION

This study revolves around the configuration of the simulation environment, aiming to provide a precise numerical simulation platform for the application of new decorative materials in different design styles. To achieve this goal, a thermodynamic simulation platform based on ANSYS Fluent and an optical simulation system based on COMSOL Multiphysics are built. By setting boundary conditions to match the actual space scale and light intensity, a virtual experimental environment that can reflect the real physical process is constructed. The configuration of the simulation environment not only includes the establishment of the geometric model but also involves the setting of multi-physics control equations, the definition of material properties, and the application of initial and boundary conditions. Among them, the geometric model is designed based on typical indoor space parameters, and the size range covers different scales from a single functional area to a complete building unit. The thermodynamic simulation part uses the finite volume method to discretize the control equations and selects the second-order implicit time integration format to ensure the calculation accuracy. In the solution process, the pressure-velocity coupling uses the SIMPLE (Semi-Implicit Method for Pressure-Linked Equations) algorithm, and the second-order upwind difference scheme is used to process the spatial discretization to ensure the resolution of the flow field and temperature field. In terms of optical simulation, the ray tracing model is built on the COMSOL Multiphysics platform. Its core is to describe the propagation path and energy distribution of light on complex surface structures. The model solves the characteristic equation to determine the refraction and reflection behavior of light between different medium interfaces. At the same time, the Monte Carlo method is applied to track a large number of light samples to obtain the surface diffuse reflection characteristics and light energy distribution laws in a statistical way. In addition, the correlation function between surface roughness and diffuse reflectivity is included in the modeling scope to more accurately reproduce the influence of the microstructure of the material surface on the light scattering behavior. As shown in Table 4, the core control parameters and their value ranges of material properties, mesh parameters, and time steps in multi-physics simulation are systematically defined. Material property parameters include density, specific heat capacity, thermal conductivity, and emissivity, and their numerical range covers typical physical properties from ceramic matrix composites to polymers. Among them, the wide range setting of thermal conductivity of 0.1–5.0W/(m·K) can adapt to the extreme thermal response requirements of phase change energy storage materials and aerogel insulation layers. The mesh parameters coordinately regulate the spatial discrete accuracy through the boundary layer growth rate, the minimum unit size, and the total number of grids. The gradient division of the boundary layer growth rate of 1.2–1.5 ensures the numerical stability of near-wall heat conduction. The fine control of the minimum unit size of 0.05–0.2mm meets the spatial resolution requirements of the surface roughness on the light scattering effect. The dynamic configuration of the total number of grids of 5×105–2×106 balances the computational efficiency and geometric complexity. The time step parameter adopts a non-uniform stratification strategy. The transient resolution capability of the thermal simulation step of $10^{-3}$–$10^{-2}$ s can capture the second-level thermal response process. The high dynamic range design of the optical sampling frequency of 100–500Hz ensures the time-domain convergence of the transient radiation flux during ray tracing. Through the above parameter settings, the constructed simulation environment can effectively support the subsequent functional performance verification and ecological economic analysis and provide theoretical support and technical guarantee for the optimized application of new decorative materials in environmental design styling.

**TABLE 4.** Multi-physics simulation parameter settings

| Parameter Category | Parameter Name | Numerical Range | Unit |
|---|---|---|---|
| Material Properties | Density | 800–2500 | $kg/m^3$ |
| | Specific Heat Capacity | 800–1500 | J/(kg·K) |
| | Thermal Conductivity | 0.1–5.0 | W/(m·K) |
| | Emissivity | 0.8–0.95 | - |
| Mesh Parameters | Boundary Layer Growth Rate | 1.2–1.5 | - |
| | Minimum Element Size | 0.05–0.2 | mm |
| | Total Mesh Count | $5 \times 10^5$–$2 \times 10^6$ | - |
| Time Step | Thermal Simulation Step | $10^{-3}$–$10^{-2}$ | s |
| | Optical Sampling Frequency | 100–500 | Hz |

## C. DATASET CONSTRUCTION

This study collects 245 sets of historical project data and systematically annotates and processes them. The constructed dataset not only covers the multi-dimensional parameters of material physical properties, but also includes key indicators such as style restoration: structural similarity index (SSIM), carbon emission intensity, etc., to ensure full-chain tracking from material science to design [30]. The dataset comprises 245 simulated data points generated through multi-physics coupling simulation technology with thirty-five per material system under controlled boundary conditions. This approach provided sufficient data diversity while maintaining experimental control. On this basis, an assessment system containing 12 quantitative adaptation indicators is constructed to measure the performance of new decorative materials in different design styles. These indicators not only involve the physical and chemical properties of the materials but also include multiple dimensions such as optical properties, thermal conductivity, and surface roughness. By combining these indicators with the actual application scenes in the dataset, the behavior of the material in the real environment can be more accurately predicted, thereby improving the overall design solution's reliability and applicability. Table 5 lists some key parameters and their value ranges and units. These parameters constitute important input variables of the multi-objective optimization

**TABLE 5.** Summary of material performance parameters

| Parameter | Physical Meaning | Measurement Range | Resolution |
|---|---|---|---|
| Flexural Strength | Resistance to bending forces | ≥85 MPa | 0.5 MPa |
| Color Deviation ($\Delta E$) | Degree of color difference from target value | ≤2.5 | 0.1 |
| Surface Roughness ($R_a$) | Average roughness of surface texture | 0.8–3.2 $\mu$m | 0.01 $\mu$m |
| Thermal Conductivity ($\lambda$) | Ability to conduct heat | 0.1–5.0 W/(m·K) | 0.01 W/(m·K) |
| Diffuse Reflectance ($\rho$) | Diffuse Reflectance ($\rho$) | ≥0.78 | 0.01 |

model and reflect the multi-level data integration process from microstructure to macro performance. The key performance parameters and their design thresholds are summarized in Table 5.

## V. RESULTS

### A. DRIVING MECHANISM OF MATERIAL ON STYLE EXPRESSION

To assess material-design compatibility and verify the proposed three-way collaborative framework, a multi-objective optimization model was constructed and applies 12 quantitative adaptation indicators, covering key parameters such as flexural strength, color deviation ($\Delta$E), and surface roughness. A comparative analysis of style restoration and error rate is conducted on five types of new decorative materials, including ceramic-based composites, photochromic polymers, bio-based resins, phase change energy storage materials, and superhydrophobic coatings. These indicators not only reflect the physical and mechanical properties of the materials but also reflect their comprehensive performance in optical response, tactile perception, and geometric morphology constraints. On this basis, a double Y-axis bar graph is used to intuitively present the difference in style adaptation accuracy between the traditional method and the proposed method under different material types, and the average SSIM value and the decrease in error rate are applied as a reference for the overall trend. As shown in Figure 3, the SSIM values of the proposed method on all five types of materials are significantly higher than those of the traditional method, reaching an average of 0.92, which is significantly higher than the 0.8 of the traditional method. Among them, the SSIM value of bio-based resin is the highest, reaching 0.93, indicating that it has strong adaptability in style feature mapping. In terms of error rate, the proposed method reduces the average error from 24.0% of the traditional method to 4.3%, a decrease of 19.7%. This improvement is mainly attributed to the precise modeling of the nonlinear relationship between material parameters and style characteristics by the multi-objective optimization algorithm, as well as the effective control of the $\Delta$E≤2.5 threshold, which makes the color expression closer to the design expectations. This method not only improves the accuracy of style restoration but also enhances the applicability of materials in diversified design contexts, providing theoretical support and technical guarantee for the engineering implementation of new decorative materials. The driving role of material parameters in style expression is reflected in the mapping relationship between its microstructure and spatial perception. Taking the new Chinese style as an example, it emphasizes the natural properties of the material itself and the clear presentation of the construction logic. The key indicators of the material such as surface roughness, chromaticity deviation, and diffuse reflectance directly affect the consistency of visual hierarchy and tactile feedback. Flexural strength and thermal conductivity indirectly determine the scale ratio and texture performance of the component in space by affecting the material molding method and interface treatment process. This formal language system constructed based on material performance enables the design intention to be precisely restored through a quantifiable technical path, thereby forming a material-dominated performance mechanism in the process of style shaping.

### B. DYNAMIC VERIFICATION OF FUNCTIONAL EFFECTIVENESS

In the application of new decorative materials, how to achieve a precise match between material performance and environmental design style has become a key challenge to enhance the overall spatial aesthetic expression and functional stability. The study focuses on five typical new decorative materials: ceramic-based composite materials, photochromic polymers, bio-based resins, phase change energy storage materials, and super-hydrophobic coatings. By constructing a three-way collaborative framework of "material properties-design requirements-application optimization", combined with multi-physics simulation and multi-objective optimization algorithms, the performance of thermal conductivity stability and functional redundancy control is systematically assessed. Among them, the fluctuation range of thermal conductivity reflects the response consistency of the material in a dynamic thermal environment. The lower the value, the more stable the thermal performance. Functional redundancy reflects the performance margin reserved by the material to cope with complex working conditions. The optimization goal is to compress it from the higher level under the traditional method to a more reasonable range. Figure 4 uses a double Y-axis line chart to clearly present the comparative relationship between the traditional method and the method in this paper on the above two indicators. The left Y-axis represents the fluctuation of thermal conductivity (in W/m·K), and the right Y-axis shows the functional redundancy (in %).

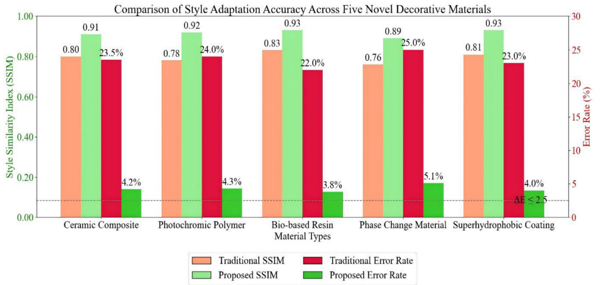


**FIGURE 3.** Comparative analysis of style adaptation accuracy of five types of new decorative materials

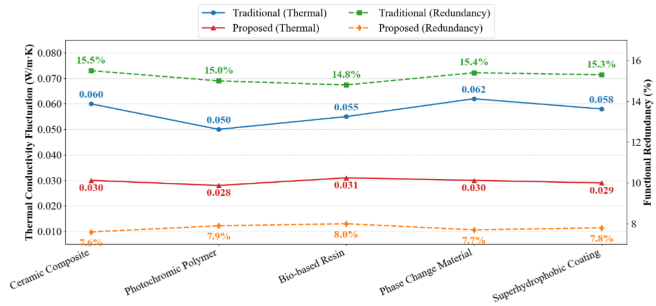


**FIGURE 4.** Comparative analysis of thermal conductivity fluctuation range an d redundancy of five types of new decorative materials

As shown in Figure 4, the thermal conductivity fluctuation ra nge of the five types of materials is relatively high under th e traditional method, while after the optimization of the m ethod in this paper, the index is compressed to about 0.03 W/m·K, a decrease of nearly half. This change shows that by applying multi-physics coupling simulation and parameterized optimization strategy, the response consistency of materials in non-steady-state thermal environment is significantly enhanced, especially in ceramic matrix composite materials and phase change energy storage materials. The functional redundancy drops from 15.2% to 7.8%, reflecting that the design redundancy is effectively controlled, avoiding the waste of resources and cost increase caused by excessive conservatism. This dual optimization effect is due to the quantitative mapping mechanism between material properties and design requirements, as well as the dynamic balance modeling from the perspective of the full life cycle, making the new decorative materials more economical and sustainable while ensuring performance. The research results verify the effectiveness of the method in improving the application efficiency of materials and provide a generalizable technical path for material selection and performance regulation in environmental design.

### C. SUSTAINABLE STYLE INNOVATION PATH

Achieving sustainable style expression requires integrating process parameter control, life cycle assessment, and design decision support into a closed-loop from material optimization to style realization. Five representative materials are selected as research objects, namely ceramic based composite materials, photochromic polymers, bio-based resin, phase change energy storage materials and super-hydrophobic coating. The “process parameters-LCA-design decision” logical chain link is constructed, and then the influence mechanism of material processing on carbon emission intensity and cost volatility is disclosed, and the promotion effect of its industrial style, naturalism and other style systems towards low carbonization is clarified. At the process parameter level, the quality of material molding is closely related to some process parameters, such as sintering temperature, curing time and coating rate, which also have a great influence on ecological and economic performance. Through the Sobol index analysis method to find out the dominant factors, and further construct the multi-dimensional parameter interaction heat base on the obtained dominant factors to quantitatively describe the carbon emission distribution characteristics of different parameter combinations. The color gradient in Figure 5 represents the carbon emission intensity under different parameter combination. The 1620°C/4.6 mL/min parameter combination marked with red circle represents the lowest emission value of 0.29 kg$CO_2$/m$^2$, which shows that the energy efficiency b alance between the material densification and coating uniformity is achieved in this process window. As shown in Figure 5, the carbon emission contribution value increases exponentially with the increase of sintering temperature. For every 120◦C increase in temperature, the emission intensity increases by 0.03– 0.07 kg$CO_2$/m$^2$, which is closely related to the crystal phase reorganization and energy consumption increase driven by high temperature. The increase in coating rate exacerbates emission fluctuations through the quadratic relationship, among which the increase in diffusion resistance after the critical point of 4.6 mL/min leads to a sudden increase in energy consumption. The optimal combination (1620◦C/4.6 mL/min) corresponds to the lowest emission intensity under parameter interaction, indicating that the medium-temperature and moderate-speed strategy achieves the coordinated optimization of environmental load and process stability by balancing material properties and process parameters, while suppressing overburning loss and ensuring film quality. On this basis, the full life cycle assessment model (LCA) is applied to include the entire process of raw material acquisition, production and manufacturing, construction application, and dismantling and recycling into the carbon footprint accounting framework. Figure 6 shows the comparative analysis of the cost volatility optimization effect and carbon emission intensity correlation of five types of new decorative materials. The bar chart clearly shows the

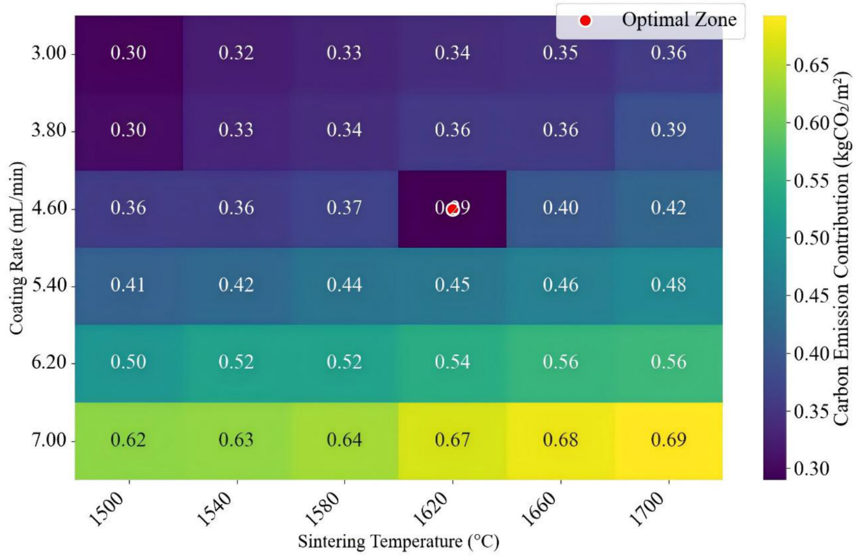


**FIGURE 5.** Heat map of the effect of process parameter interaction on carbon emission contribution

cost control effect of each material under the two methods. The red dotted line indicates the economic threshold of 4.5%, which is used to measure whether the cost fluctuation is within an acceptable range; the scatter plot further takes carbon emission intensity into consideration, with each point representing a material and the color distinguishing the type, to explore its potential impact on economic efficiency. As shown in Figure 6, all materials have achieved a significant reduction in cost volatility under the method proposed in this paper, and the values are concentrated in the range of 3.9% to 4.3%, which is lower than the set threshold. The carbon emission intensity is distributed between 1.68 and 1.78 $kgCO_2/m^2$, which is generally maintained at a low level. This result shows that the improvement in the economic efficiency of the material has not sacrificed environmental performance, and the two have a certain degree of decoupling ability. The trend of the scatter plot shows that there is no obvious positive or negative change pattern between carbon emission intensity and cost volatility. Combined with their respective distributions, there is no obvious upward or downward trend line. It can be considered that the correlation between the two is weak, which supports the feasibility of independently processing economic and ecological indicators in the multi-objective optimization framework. Further analysis shows that the mapping relationship between the above process parameters and LCA indicators can effectively support the quantitative guidance of design decisions. By embedding carbon emission intensity and cost volatility as constraints into the mixed integer programming algorithm, the optimal solution with both low carbon emissions and high economic stability is screened out to ensure that the material selection not only meets the spatial aesthetics and functional requirements but also has predictable ecological and economic performance. This path strengthens the driving role of materials as style media in the dual dimensions of ecological perception and visual expression, and turns the style shaping process from experience-oriented to data-driven, this is especially relevant for the textile engineering sector, where the precision of material performance is critical for functional aesthetics, showing stronger technical adaptability and aesthetic expansion potential in the design context of industrial style, naturalism, and other sustainable development.

### *D. MULTI-PHYSICS COUPLING EFFECT*

In the process of shaping the environmental design style, the coupling relationship between the surface physical properties and optical properties of new decorative materials has become a key factor affecting the visual quality of space. The study focuses on five typical materials: ceramic-based composite materials, photochromic polymers, bio-based resins, phase change energy storage materials, and super-hydrophobic coatings. By constructing a quantitative relationship curve between surface roughness (Ra) and diffuse reflection uniformity (expressed as the coefficient of variation value), the optical response characteristics of different material systems under the action of multi-physics are revealed. Due to the differences in microstructure and surface morphology, each material exhibits different scattering behaviors under different roughness conditions. The CV (Coefficient of Variation) value is a statistical indicator for measuring the consistency of diffuse reflection distribution. The lower the value, the more uniform the light distribution is, which is more conducive to improving the visual comfort of the space. The curves in Figure 7 correspond to the CV performance of different materials in the range of 0.2 to 5.6 $\mu$m as the surface roughness changes. As shown in Figure 7, the change trend of diffuse reflection uniformity of five types of new decorative materials under different surface roughness conditions. Among them, the horizontal axis is the surface roughness Ra ($\mu$m), and the vertical axis is the CV value. The marked points represent the

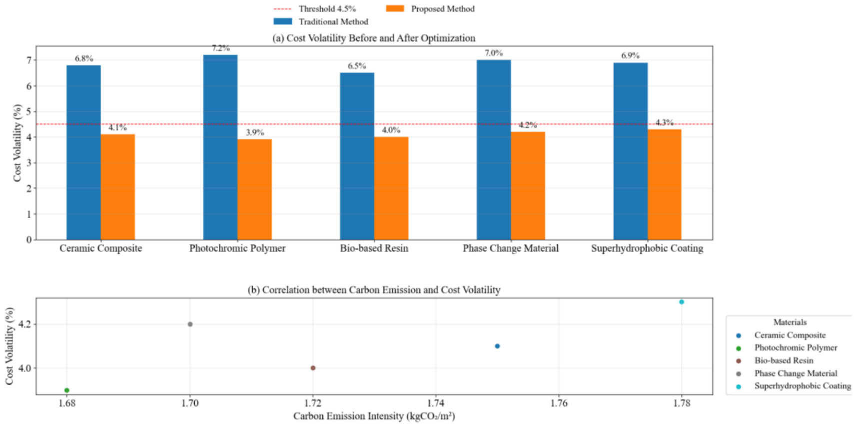


**FIGURE 6.** Comparative analysis of the correlation between cost volatility optimization effect and carbon emission intensity of five types of new decorative materials. (a) .Cost volatility of different methods; (b) .Correlation between carbon emission and cost volatility

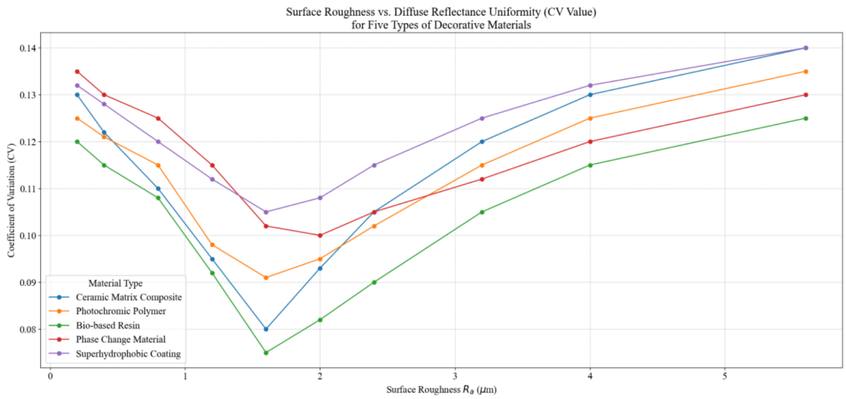


**FIGURE 7.** Curve of the influence of surface roughness on diffuse reflection uniformity of five types of new decorative materials

optimal scattering uniformity position of each material. Ceramic-based composites and bio-based resins reach the lowest CV values near Ra=1.6 $\mu$m, which are 0.08 and 0.075, respectively, indicating that the microstructure at this scale has the best adaptability to light field regulation. The minimum CV values of photochromic polymers and phase change energy storage materials appear at 1.6 $\mu$m and 2.0 $\mu$m, respectively, showing a certain degree of deviation, reflecting the difference in sensitivity of their surface energy states or thermal response mechanisms to roughness. The minimum CV value of the superhydrophobic coating appears at Ra=1.6 $\mu$m, but its value is higher than that of other materials, indicating that its interface structure has a weak ability to regulate scattering uniformity, which may be related to the synergistic effect of surface chemical inertness and multi-scale structure. This phenomenon is closely related to the surface chemical composition of the material itself, the arrangement of micro-nanostructures, and their interaction mechanism with incident light, further confirming the nonlinear mapping relationship between material science parameters and optical properties. The diversity of curve forms also verifies the differentiated trend of material functionalization paths and provides data support for the collaborative design of decorative materials between style expression and performance optimization.

## VI. CONCLUSION

This paper reveals the core position of new decorative materials (including textile-derived media) as style media and proposes a "material characteristics-design requirements-application optimization" framework to shift their role from passive adaptation to active driver. The causal relationship between material performance and aesthetic expression is clarified in typical style systems such as industrial style and naturalism. Based on thermodynamic simulation, light environment simulation technology and life cycle assessment model, this study systematically analyzes and experimentally verifies five types of new decorative materials consisting of various fiber structures and composite textures. The research results have verified that as the style media, materials play an important role in enhancing style restoration. The average style structural similarity index (SSIM) is 0.92, and the style adaptation error rate decreases from 24.0% of the traditional method to 4.3%. There is obvious potential for style innovation in mainstream styles such as industrial style and naturalism. The functional efficiency redundancy is reduced from 15.2% to 7.8%, and the carbon emission intensity is controlled within the limit of $1.8kgCO_2/m^2$. Although this study has achieved a break-through in style shaping driven by materials, the stability of material quality performance in dynamic environmental loads and universality in different style contexts still need to be strengthened. Especially, the long-term performance verification in style system such as industrial style and naturalism should be the key exploration of the follow-up work. In addition, the long short term memory networks will be embedded into the predictive model for dynamic optimization, more material applications will be extended, and more interdisciplinary integration will be promoted in the future work to achieve sustainable environmental design, and the innovative development of the textile-based decorative industry.

## AUTHOR CONTRIBUTIONS

Qian Lyu: Writing - Original Draft, Data Curation
Zhidong Huang: Conceptualization, Methodology

## CONFLICTS OF INTEREST

These no potential competing interests in our paper. And all authors have seen the manuscript and approved to submit to your journal. We confirm that the content of the manuscript has not been published or submitted for publication elsewhere.

## FUNDING

This research received no external funding.

## ACKNOWLEDGEMENTS

The author acknowledges the support and contributions that facilitated the completion of this work.

## REFERENCES

[1] Y. Mao, "Influence of material and decoration on design style, aesthetic performance, and visual attention in Chinese-style chairs," Forest Products Journal, vol. 74, no. 3, pp. 220-232, 2024, doi: 10.13073/FPJ-D-24-00017.
[2] X. Wang, Y. Zhong, F. Zhu, and J. Huang, "Digital industrial design method in architectural design by machine learning optimization: towards sustainable construction practices of geopolymer concrete," Buildings, vol. 14, no. 12, pp. 3998-4030, 2024, doi: 10.3390/buildings14123998.
[3] H. Gonul, "The unacknowledged status of applied ornament in contemporary architecture," VLC Arquitectura. Research Journal, vol. 12, no. 1, pp. 9-25, 2025, doi: 10.4995/vlc.2025.22698.
[4] Y. Zhang, Y. Song, and J. Luo, "The effect of sustainable and natural looking on perceived aesthetics and ecofriendliness in building material evaluation," Buildings, vol. 13, no. 2, pp. 483-495, 2023, doi: 10.3390/buildings13020483.
[5] Z. Wu, "Performance analysis of new energy-saving and environment-friendly materials for building decoration based on the whole life cycle," Journal of Experimental Nanoscience, vol. 18, no. 1, pp. 2170358-2170376, 2023, doi: 10.1080/17458080.2023.2170358.
[6] H. Wu, W. Zhou, K. Chen, L. Zhang, Z. Zhang, Y. Li, et al., "Carbon emissions assessment for building decoration based on life cycle assessment: a case study of office buildings," Sustainability, vol. 15, no. 19, pp. 14055-14073, 2023, doi: 10.3390/su151914055.
[7] M. Reyhani, E. Santolini, P. Tassinari, and D. Torreggiani, "Environmental assessment of design choices of green walls based for materials combination and plants," The International Journal of Life Cycle Assessment, vol. 28, no. 9, pp. 1078-1091, 2023, doi: 10.1007/s11367-023-02181-x.
[8] M. Ghanbari, "Environmental impact assessment of building materials using life cycle assessment," Journal of Architecture, Environment and Structural Engineering Research, vol. 6, pp. 11-22, 2023, doi: 10.30564/jaeser.v6i4.5964.
[9] V. Cascione, M. Roberts, S. Allen, C. Charbel, D. Maskell, B. Dams, et al., "Evaluating environmental impacts of bio-based insulation materials through scenario-based and dynamic life cycle assessment," The International Journal of Life Cycle Assessment, pp. 1-20, 2025, doi: 10.1007/s11367-024-02425-4.
[10] L. Zhang, H. Wu, X. Wang, F. Wu, Z. Ding, L. Song, et al., "Quantification of carbon emissions of building decoration processes," Buildings, vol. 14, no. 11, pp. 3570-3592, 2024, doi: 10.3390/buildings14113570.
[11] X. Wang, F. Cui, L. Cui, and D. Jiang, "Research on a multi-objective optimization design for the durability of high-performance fiber-reinforced concrete based on a hybrid algorithm," Coatings, vol. 13, no. 12, pp. 2054-2073, 2023, doi: 10.3390/coatings13122054.
[12] G. Yao, R. Li, and Y. Yang, "An improved multi-objective optimization and decision-making method on construction sites layout of prefabricated buildings," Sustainability, vol. 15, no. 7, pp. 6279-6302, 2023, doi: 10.3390/su15076279.
[13] Q. Diao, Y. Zeng, and J. Chen, "The applications and latest progress of ceramic 3D printing," Additive Manufacturing Frontiers, vol. 3, no. 1, pp. 200113-200137, 2024, doi: 10.1016/j.amf.2024.200113.
[14] B. Y. Karlinskii and V. P. Ananikov, "Recent advances in the development of green furan ring-containing polymeric materials based on renewable plant biomass," Chemical Society Reviews, vol. 52, no. 2, pp. 836-862, 2023, doi: 10.1039/D2CS00773H.
[15] H. Y. Chen, Z. Y. Chen, M. Mao, Y. Y. Wu, F. Yang, L. Gong, et al., "Self-adhesive polydimethylsiloxane foam materials decorated with MXene/cellulose nanofiber interconnected network for versatile functionalities," Advanced Functional Materials, vol. 33, no. 48, pp. 2304927-2304939, 2023, doi: 10.1002/adfm.202304927.
[16] Y. Lu, W. Wu, X. Geng, Y. Liu, H. Zheng, and M. Hou, "Multi-objective optimization of building environmental performance: an integrated parametric design method based on machine learning approaches," Energies, vol. 15, no. 19, pp. 7031-7054, 2022, doi: 10.3390/en15197031.
[17] I. de Paula Salgado, F. Conrad, C. Signorini, C. Günther, S. Ihlenfeldt, and V. Mechtcherine, "Integrating life cycle assessment (LCA) and machine learning for sustainable designs: a case study on protective layers made of mineral-bonded fiber-reinforced composites," The International Journal of Life Cycle Assessment, pp. 1-20, 2025, doi: 10.1007/s11367-025-02454-7.
[18] Y. Liu, "Ecological Graphic Design: Innovative Application of Environmentally Respectful Materials and Design Language," Journal of Education, Humanities and Social Sciences, vol. 59, no. 1, pp. 126-155, 2025, doi: https://doi.org/10.54097/8wqrjz25.
[19] B. Altay and E. Salcı, "Exploring designers' finishing materials selection for residential interior spaces," Architectural Engineering and Design Management, vol. 20, no. 2, pp. 269-286, 2024, doi: 10.1080/17452007.2023.2181753.
[20] W. Nilam, "Fusion of ornamental art and architectural design: exploring the interplay and creation of unique spatial experiences," Studies in Art and Architecture, vol. 2, no. 3, pp. 10-27, 2023, doi: 10.56397/SAA.2023.09.03.
[21] Y. Zhou, V. W. Y. Tam, and K. N. Le, "Developing a multi-objective optimization model for improving building's environmental performance over the whole design process," Building and Environment, vol. 246, pp. 110996-111011, 2023, doi: 10.1016/j.buildenv.2023.110996.
[22] N. Izadinia, E. Ramyar, M. Alzayer, S. Carr, G. Cusatis, V. Dwivedi, et al., "A versatile optimization framework for sustainable post-disaster building reconstruction," Optimization and Engineering, vol. 24, no. 3, pp. 2079-2114, 2023, doi: 10.1007/s11081-022-09766-9.
[23] R. Talami, J. Wright, and B. Howard, "Evaluating the effectiveness, reliability and efficiency of a multi-objective sequential optimization approach for building performance design," Energy and Buildings, vol. 329, pp. 115242-115287, 2025, doi: 10.1016/j.enbuild.2024.115242.
[24] M. A. DeRousseau, J. R. Kasprzyk, and W. V. Srubar, "Multi-objective optimization methods for designing lowcarbon concrete mixtures," Frontiers in Materials, vol. 8, pp. 680895-680908, 2021, doi: 10.3389/fmats.2021.680895.
[25] M. Schwartz, "Human centric accessibility graph for environment analysis," Automation in Construction, vol. 127, pp. 103557-103578, 2021, doi: 10.1016/j.autcon.2021.103557.
[26] H. E. Wray, S. Luzzi, P. D'Arrigo, and G. Griffini, "Life cycle environmental impact considerations in the design of novel biobased polyurethane coatings," ACS Sustainable Chemistry & Engineering, vol. 11, no. 21, pp. 8065-8074, 2023, doi: 10.1021/acssuschemeng.3c00619.
[27] K. Theilig, B. Lourenço, R. Reitberger, and W. Lang, "Life cycle assessment and multi-criteria decision-making for sustainable building parts: criteria, methods, and application," The International Journal of Life Cycle Assessment, vol. 29, no. 11, pp. 1965-1991, 2024, doi: 10.1007/s11367-024-02331-9.

[28] S. Liang, "Optimization of thermal performance in green building materials based on thermodynamic principles," International Journal of Heat & Technology, vol. 42, no. 3, pp. 739-739, 2024, doi: 10.18280/ijht.420303.

[29] Harshalatha, S. Patil, and P. G. Kini, "A review on simulation based multi-objective optimization of space layout design parameters on building energy performance," Journal of Building Pathology and Rehabilitation, vol. 9, no. 1, pp. 69-86, 2024, doi: 10.1007/s41024-024-00425-3.

[30] D. Yang, C. Vezzoli, and H. Su, "Comprehensive life cycle assessment of 25 furniture pieces across categories for sustainable design," Scientific Reports, vol. 15, no. 1, pp. 13968-13984, 2025, doi: 10.1038/s41598-024-84025-8.